ORIGINAL ARTICLE

[18F]MAGL-4-11 positron emission tomography molecular imaging of monoacylglycerol lipase changes in preclinical liver fibrosis models

Tuo Shao[a,b,†], Zhen Chen[a,†], Jian Rong[a,†], Vasily Belov[a,c],
Jiahui Chen[a], Andre Jeyarajan[b], Xiaoyun Deng[a], Hualong Fu[a],
Qingzhen Yu[a], Steve H. Rwema[b], Wenyu Lin[b], Mikhail Papisov[a,c],
Lee Josephson[a], Raymond T. Chung[b,*], Steven H. Liang[a,*]

[a]Division of Nuclear Medicine and Molecular Imaging, Department of Radiology, Massachusetts General Hospital and Harvard Medical School, Boston, MA 02114, USA
[b]Liver Center and Gastrointestinal Division, Department of Medicine, Massachusetts General Hospital, Harvard Medical School, Boston, MA 02114, USA
[c]Shriners Hospitals for Children-Boston Boston, MA 02114, USA

Abstract Monoacylglycerol lipase (MAGL) is a pivotal enzyme in the endocannabinoid system, which metabolizes 2-arachidonoylglycerol (2-AG) into the proinflammatory eicosanoid precursor arachidonic acid (AA). MAGL and other endogenous cannabinoid (EC) degrading enzymes are involved in the fibrogenic signaling pathways that induce hepatic stellate cell (HSC) activation and ECM accumulation during chronic liver disease. Our group recently developed an 18F-labeled MAGL inhibitor ([18F]MAGL-4-11) for PET imaging and demonstrated highly specific binding in vitro and in vivo. In this study, we determined [18F]MAGL-4-11 PET enabled imaging MAGL levels in the bile duct ligation (BDL) and carbon tetrachloride (CCl4) models of liver cirrhosis; we also assessed the hepatic gene expression of the enzymes involved with EC system including MAGL, NAPE-PLD, FAAH and DAGL that as a function of disease severity in these models; [18F]MAGL-4-11 autoradiography was performed to assess tracer binding in frozen liver sections both in animal and human. [18F]MAGL-4-11 demonstrated reduced PET signals in early stages of fibrosis and further significantly decreased with disease progression compared with control mice. We confirmed MAGL and FAAH expression decreases with fibrosis

severity, while its levels in normal liver tissue are high; in contrast, the EC synthetic enzymes NAPE-PLD and DAGL are enhanced in these different fibrosis models. *In vitro* autoradiography further supported that [^{18}F]MAGL-4-11 bound specifically to MAGL in both animal and human fibrotic liver tissues. Our PET ligand [^{18}F]MAGL-4-11 shows excellent sensitivity and specificity for MAGL visualization *in vivo* and accurately reflects the histological stages of liver fibrosis in preclinical models and human liver tissues.

1. Introduction

Liver fibrosis is a consequence of sustained injury from a variety of origins, including chronic viral infection, cholestatic liver disease, alcohol abuse, and nonalcoholic steatohepatitis (NASH)[1]. Fibrosis of the liver is associated with the excessive extracellular matrix (ECM) protein accumulation and formation of a fibrous scar[2]. As scarring progresses, subsequent growth of nodules from regenerating hepatocytes results in ultimately liver cirrhosis, which is the end consequence of progressive fibrosis and attended by high morbidity and mortality. Because patients with liver fibrosis are at high risk for the development of cirrhosis, the use of non-invasive imaging modalities such as molecularly targeted positron emission tomography (PET) to detect early stage liver fibrosis and/or monitor targeted therapy at the cellular level may be of great translational value[3]. Until now, liver biopsy has been the gold standard for identifying liver fibrosis but has well-known limitations. Other procedures include ultrasonography and elastography still suffer from low sensitivity and specificity[4]. Accordingly, the development of novel PET imaging agents with alternative binding mechanisms and/or differential signaling transduction pathways is of particular interest for the physiologic processes and treatment of liver fibrosis.

Recent clinical observations and experimental studies have demonstrated that the endocannabinoid system, including cannabinoid receptors, endogenous cannabinoid (EC) ligands and degrading enzymes, such as monoacylglycerol lipase (MAGL) and fatty acid amide hydrolase (FAAH), are involved in the fibrogenic signaling pathways that induce hepatic stellate cell (HSC) activation and ECM accumulation during chronic liver disease[5−13]. However, the contribution of MAGL to fibrosis in chronic liver injury has been poorly understood. MAGL is a pivotal enzyme in the endocannabinoid system, which metabolizes 2-arachidonoylglycerol (2-AG) into the proinflammatory eicosanoid precursor arachidonic acid (AA). 2-AG, a natural ligand for cannabinoid receptors, is likely to be a fibrogenic mediator because its hepatic levels are selectively increased in preclinical liver fibrosis models. In addition, recent studies have demonstrated that MAGL plays an important role in liver injury/inflammation, liver steatosis and liver fibrosis by modulating endocannabinoid receptor (CB1/2) signaling or eicosanoid synthesis[11−14]. Giannone et al.[9] found that hepatic MAGL gene expression was downregulated in carbon tetrachloride (CCl$_4$) induced liver fibrosis, and CB1 receptor antagonists upregulated CB2, reversed EC enzyme MAGL levels and induced fibrosis regression. Therefore, these findings suggest that MAGL can become an important therapeutic drug target for liver disease.

Our group recently developed an ^{18}F-labeled MAGL inhibitor ([^{18}F]MAGL-4-11) for PET imaging and demonstrated highly specific binding *in vitro* and *in vivo*[15]. In this work, the goals of our investigation were (i) to determine the hepatic gene expression of the enzymes involved with EC system as a function of disease severity in the bile duct ligation (BDL) and carbon tetrachloride (CCl$_4$) models of liver cirrhosis; (ii) to show that [^{18}F]MAGL-4-11 PET enabled imaging MAGL in these models and, (iii) to demonstrate that [^{18}F]MAGL-4-11 PET uptake and binding correlated with the degree of liver cirrhosis in pre-clinical and clinical liver sections. To our delight, our results indicate that [^{18}F]MAGL-4-11 PET is able to image MAGL function and expression *in vivo* in preclinical mouse models and human tissues of liver fibrosis, the results of which would improve our understanding of its role in liver pathology and facilitate drug discovery for liver fibrosis treatment.

2. Materials and methods

2.1. Experimental protocol of liver fibrosis

Carbon tetrachloride (CCl$_4$ treatment): CD1 male mice at 10 weeks of age were given intraperitoneal (i.p.) injection of carbon tetrachloride biweekly (CCl$_4$, Sigma) with the following formulation and dose (20% solution of CCl$_4$ in olive oil mixture; injection dose 0.2 mL/kg) for 12 weeks. Control mice were treated with the same isovolumetric dose of vehicle (olive oil) as i.p. injection. Bile duct ligation (BDL) surgery: the common bile duct was mobilized and dissected between two sutures following midline laparotomy. Sham mice treated with midline laparotomy without, scission procedure. All procedures were approved by the Massachusetts General Hospital IACUC committee.

2.2. Micro-PET/CT imaging scanning and analysis

[^{18}F]MAGL-4-11 synthesis was performed at MGH Cyclotron Facility. PET imaging and quantification were performed as previously described. Briefly, control, CCl$_4$ and BDL groups were anesthetized with 5% isoflurane gas before 0.1 cc of 3.5−3.7 MBq of [^{18}F]MAGL-4-11 intravenous injection, and kept thereafter with 1%−2% (v/v) isoflurane. PET/CT was performed for 30 min after intravenous injection of tracer on a Focus 220 preclinical PET system (Siemens) and the CereTom NL 3000 CT scanner (Neurologica). PET/CT image was co-registered semi-automatically using ASIProVM and Inveon Research Workplace (Siemens Medical Solutions). The magnitude of hepatic [^{18}F]MAGL-4-11

activation was expressed as %ID/g which was defined as the average [^{18}F]MAGL-4-11 activity in each volume of interest (VOIs) divided by injected dose.

2.3. Liver histology

The paraffin liver tissues were prepared in 5 μm sections and stained with hematoxylin and eosin according to the manufacturer's procedure (Sigma). Under blinding protocols (BLD and sham samples were unknown to experimenters), the extent of necrosis and inflammation was examined. To detect hepatic fibrosis accumulation, Sirius red staining was conducted with paraffin liver sections with the use of Sirius red F35B to stain collagen, hematoxylin was used counterstained nuclear.

2.4. Measurement of hydroxyproline

The levels of liver hydroxyproline were determined using the Hydroxyproline Assay Kit (Sigma, St. Louis, MO, USA) and the hydroxyproline content was expressed as μg/g of liver.

2.5. Immunofluorescent staining

Immunofluorescent staining was performed as previously described[16]. Following deparaffinization, antigen retrieval buffer was added to the microwaveable vessel. Liver sections were treated with PBS (containing 1% BSA) and 0.3% Triton X-100 after antigen recovery. Primary antibodies anti-MAGL (Abcam), anti-α-SMA (Abcam), anti-CD45 (Abcam) and anti-CD68 (Cell Signaling) were incubated with sections at 4 °C overnight. Sections were rinsed by PBS and secondary antibodies with Alexa Fluor 488 or Alexa Fluor 594 (Abcam) were incubated for 60 min at room temperature. VECTASHIELD antifade mounting medium with DAPI (Vector Labs) was used for DAPI counterstain and mounting.

2.6. RNA extraction, cDNA synthesis and qPCR

Total RNA was extracted by Qiagen's RNeasy Mini kit. cDNA was synthesized using the RT-for-PCR kit. Gene expression levels were measured using ABI QuantStudio three system (Applied Biosystems) and Power Up SYBR green master mix (Thermo Fisher Scientific). The primer sequences are listed in Supporting Information Table S1. The results were processed as relative values of mRNA levels based on ΔΔCT method.

2.7. Western blot analysis

Proteins were extracted using radioimmunoprecipitation assay (RIPA) buffer and a protease inhibitor cocktail (Sigma Life Science) from liver tissues and each concentration was measured by BCA Protein Assay Kit (Thermo scientific). Protein samples were loaded on precast gels and blotted onto Blot two Dry Blotting System (Thermo scientific). The membranes were treated with 5% skim milk and incubated with the different primary antibodies anti-MAGL (Abcam), anti α-SMA (Abcam) and anti-β-actin (Sigma Life Science) at 4 °C overnight. After TBST wash, membranes reacted with secondary antibodies. Protein bands were quantified using ChemiDoc Touch Gel Imaging System (Bio-Rad). The immunoblot band analysis for determining intensity was imaged using Image lab (Bio-Rad).

2.8. Autoradiography

Frozen sections of OCT-embedded liver tissue were cut (20 μm thick sections) using cryostat (Microm Typ HM 500; Microm). Briefly, frozen sections were activated in Tris-HCl (pH 7.4), then incubated with [^{18}F]MAGL-4-11 in the buffer. Sections were exposed to storage phosphor screens (GE) for 2 h. The screen was read with a GE Typhoon system at a resolution of 20 μm × 20 μm. Autoradiographic images were then analyzed using Image Quant image analysis software (Molecular Dynamics).

2.9. Patients liver specimens

Liver specimens were obtained from patients diagnosed with liver fibrosis (F1 $n = 3$ and F2 $n = 3$) and health patients (F0 $n = 3$). This study was approved by the IRB of Massachusetts General Hospital (USA, Table S1).

2.10. Statistical analysis

The results are expressed as means ± SE and statistics were analyzed with Student's t-tests or one-way ANOVA with Tukey's post hoc test. Differences were considered to be significant at $^*P < 0.0$, $^{**}P < 0.01$ or $^{***}P < 0.001$, $n = 3-6$/group.

3. Results

3.1. The development of hepatic injury and fibrosis in distinct mouse models

Morphological analysis by H&E staining demonstrated that the administration of CCl$_4$ to mice caused hepatic inflammation with hepatocyte ballooning and aggregation of lymphocytes at 6 weeks, and irregular necrosis at 12 weeks (Fig. 1A). The liver fibrosis stages were determined by Sirius red (SR) staining: the mild stage of the fibrosis process (1−6 weeks) was characterized by a mild form consists of deposition of collagen fibers in the pericentral lobular region; the severe stage of fibrosis process (6−12 weeks) was characterized by an advanced accumulation of broad collagen fibers (Fig. 1A and C). For the BDL-induced biliary fibrosis model, mice presented with remarkable liver inflammation and fibrosis. The accumulation of inflammation and collagen was noted in livers at 10 and 21 days after BDL treatment (Fig. 1B). SR staining showed an increase positive collagen area at 10 and 21 days after BDL (Fig. 1B and C). These were also supported by the findings that serum hydroxyproline levels were increased in CCl$_4$ and BDL mice (Fig. 1D).

3.2. PET/CT imaging and quantitation of [^{18}F]MAGL-4-11 in fibrotic livers

To determine MAGL levels during fibrosis, MAGL-PET/CT were carried out from 0 to 30 min following [^{18}F]MAGL-4-11 injection in 6- & 12-week CCl$_4$-treated mice, 10-day & 21-day BDL-treated mice or normal control mice. Fig. 2A represents summed transverse PET/CT images (0−30 min) of normal, 6-week CCl$_4$ & 12-week CCl$_4$ livers, while Fig. 2C shows similar images for sham, 10- & 21-day BDL livers. The tracer uptake was gradually declined with disease progression. Declined uptakes of [^{18}F]MAGL-4-11 were found with mild fibrosis in 6-week CCl$_4$-treated and 10-day BDL-treated livers compared with controls/shams.
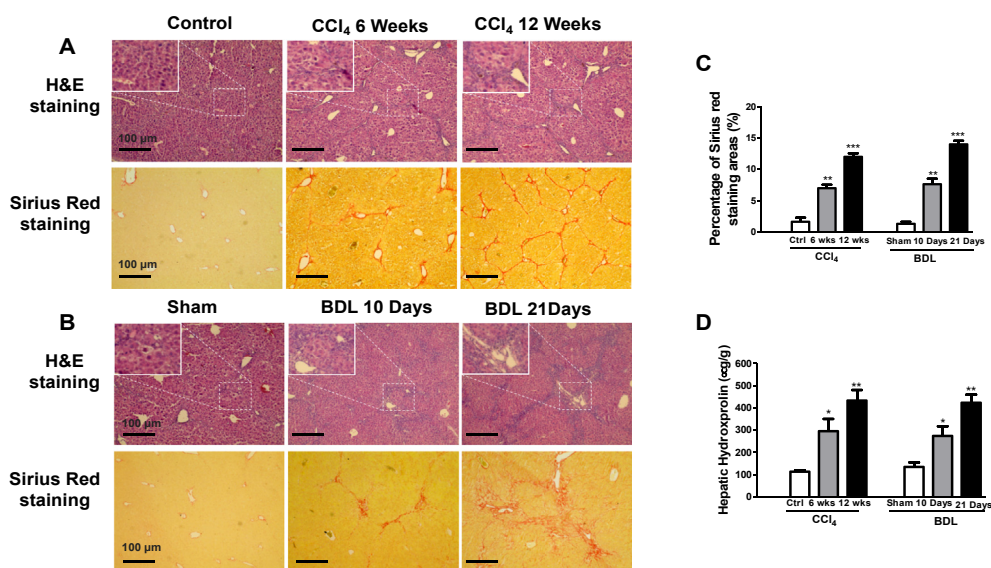
Figure 1 Pathological features of liver fibrosis in the CCl4 or BDL model. (A, B) Representative images of hemaxotoxylin and eosin (H&E) and Sirius red staining of liver sections in mice exposed to CCl4 (6 and 12 weeks) and BDL (10, 21 days). Scale bars: 100 μm, original magnifications: H&E 10 ×, SR 10 ×. (C) The quantification of the Sirius red collagen positive fibrosis area in sections. *P* values are relative to control/sham. (D) Serum hydroxyproline levels for CCl4 and BDL mice. Graph represents mean ± SEM. $*P < 0.05$, $**P < 0.01$, and $***P < 0.001$, $n = 6$ animal/group. ANOVA, analysis of variance.

Significantly lower levels of radioactivity were observed in 12-week CCl4-treated and 21-day BDL-treated livers. Time-activity curves (TACs) were analyzed by drawn interest area for [18F]MAGL-4-11 in the livers between 0 and 30 min. Fig. 2B and D shows TACs which radioactivity is expressed as %injected dose per gram (%ID/g).

3.3. Expression of MAGL protein and key enzymes in EC metabolism

To further confirm the PET imaging results, the relationship between hepatic MAGL level and fibrosis extent, MAGL proteins level were conducted by Western blots in the CCl4 and BDL models (Fig. 3A and B). CCl4 and BDL treatment groups had weaker hepatic MAGL expression compared with control and sham groups. With disease progression, MAGL expression was significantly decreased in both CCl4 and BDL-treated livers.

To study the underlying mechanism of liver fibrosis associated with MAGL, gene expression of MAGL, FAAH, diacylglycerol lipase (DAGL), phospholipase D (PLD) and cannabinoid receptor type I (CB1) were analyzed by RT-PCR (Fig. 3C). gene expression of the hepatic degradative enzymes MAGL and FAAH gene expression was decreased after CCl4 and BDL treatment. In contrast, mRNA levels of the biosynthetic enzymes DAGL,
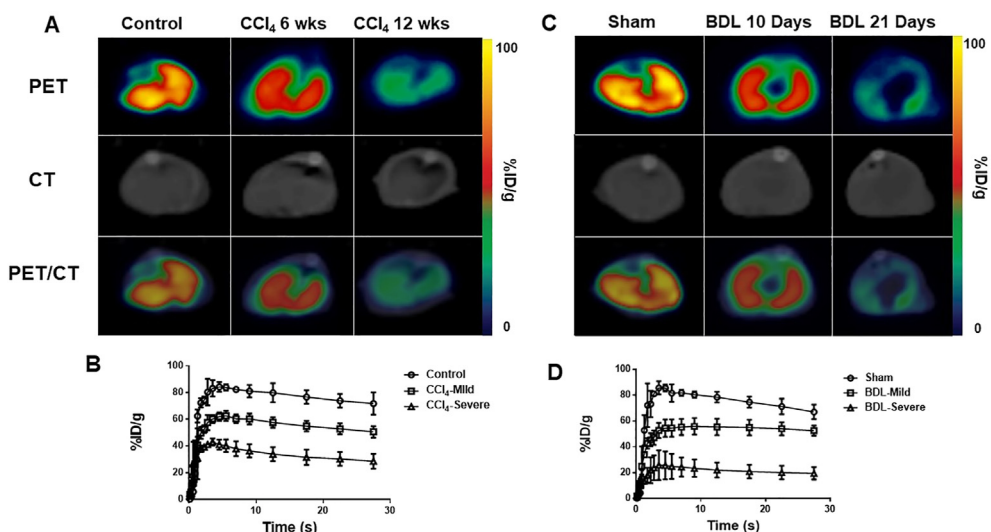

Figure 2 Representative PET/CT images of livers in CCl4 and BDL mice. (A) Representative transverse PET images of [18F]MAGL-4-11 in 6-week & 12-week CCl4 and control mice. (B) Time−activity curves (TACs) of [18F]MAGL-4-11 for CCl4 treated livers from 0 to 30 min after injection, $n = 4$ animal/group. (C) Representative transverse PET images of [18F]MAGL-4-11 in 10 & 21-day BDL and sham mice. (D) Time−activity curves (TACs) of [18F]MAGL-4-11 for BDL treated livers from 0 to 30 min after injection, $n = 4$ animal/group.
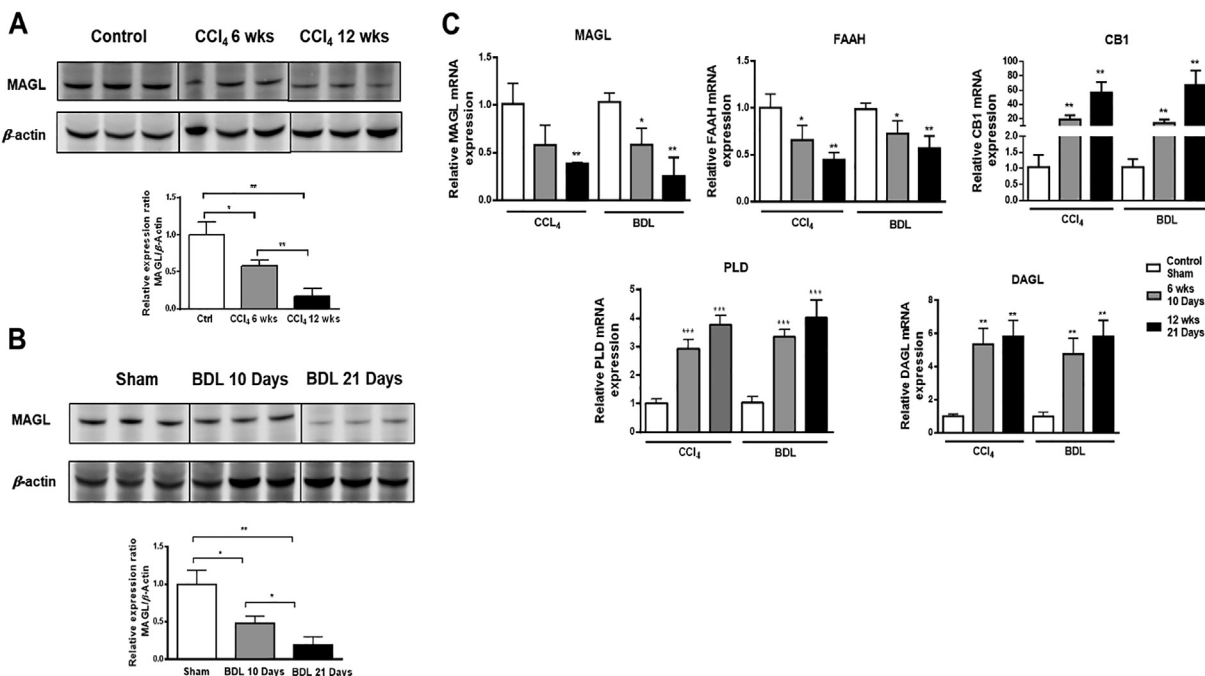
Figure 3 Hepatic expression of MAGL and key genes in CCl_4 and BDL models. (A, B) The MAGL protein level was examined in liver tissues from CCl_4 and BDL. (C) Hepatic mRNA expression levels of MAGL, FAAH, CB1, PLD and DAGL by RT-PCR. *P* values are relative to control/sham. Graph represents mean ± SEM. *$P < 0.05$, **$P < 0.01$, and ***$P < 0.001$, $n = 6$ animal/group. ANOVA, analysis of variance.

NAPE-PLD were upregulated during disease progression in both models. Finally, gene expression of the CB1 receptor were clearly upregulated in fibrotic livers.

3.4. [¹⁸F]MAGL-4-11 autoradiography and MAGL distribution in mouse fibrotic livers

To evaluate that our PET tracer, [¹⁸F]MAGL-4-11, bound hepatic MAGL as predictor in liver fibrosis models, [¹⁸F]MAGL-4-11 autoradiography binding was correlated with MAGL expression by immunofluorescent staining (Fig. 4). In the CCl_4 (Fig. 4A) and BDL model (Fig. 4B), radioactivity was decreased with fibrosis progression and consistent with immunofluorescent staining for MAGL levels (red). Immunofluorescence for α-SMA expression (green) tracked with fibrosis progression [¹⁸F]MAGL-4-11 radioactivity from CCl_4 and BDL liver sections was strongly correlated with MAGL protein expression (Fig. 4C), which was assessed by analysis of the same sections (Fig. 4D, $R^2 = 0.967$, $P < 0.001$, CCl_4; $R^2 = 0.907$, $P < 0.001$, BDL).

3.5. [¹⁸F]MAGL-4-11 autoradiography and MAGL distribution in human specimens

To further verify whether our findings are consistent with clinical situation, we performed autoradiography studies of [¹⁸F]MAGL-4-11 on human liver specimens obtained from normal and patients with hepatic fibrosis. Fig. 5A shows the [¹⁸F]MAGL-4-11 autoradiography binding in liver sections, with a decrease radioactivity sensitivity from mild to severe fibrosis. Fig. 5A also exhibits the results of MAGL immuno-fluorescence (red) and α-SMA (green) staining of liver samples indicated in the white box (top). Liver fibrotic and cirrhotic patients showed the expected hepatic α-SMA expression upregulation, but downregulation of MAGL expression

was observed with disease progression, confirmed by the results obtained by autoradiography. Uptake of [¹⁸F]MAGL-4-11 in human liver fibrosis samples decreased with reduced MAGL expression in a linear manner, as measured by [¹⁸F]MAGL-4-11 autoradiographic and MAGL fluorescence signal quantification ($R^2 = 0.967$, $P < 0.001$, Fig. 5B and C).

4. Discussion

The EC system is involved in the ECM deposition during chronic liver diseases, and MAGL—one of the most important endocannabinoid-degrading enzymes—plays a critical role in EC metabolism[17,18]. There has been a growing body of evidence implicating MAGL as an antifibrotic drug target. Inhibition of MAGL produced a profound treatment effect towards hepatic inflammation and fibrosis in different experimental models of chronic liver injury[11−13,19]. Therefore, clinically relevant imaging agents and modalities for direct and noninvasive imaging of MAGL are an urgent topic of great interest and importance. To the best of our knowledge, we demonstrate the first study that systematically validates MAGL-targeted PET/CT imaging of liver fibrosis in preclinical liver fibrosis models and clinical specimens. Our study is novel, since it demonstrates MAGL function and expression changes associated with liver fibrosis progression using a non-invasive and longitudinal imaging method. These findings have been confirmed by histopathology, immunohistochemistry, and autoradiography in preclinical and clinical fibrotic liver specimens.

To date, there have been few reports studying hepatic MAGL gene and protein expression in liver fibrosis mouse models[9]; therefore, we utilized two widely-used murine fibrosis models, namely the CCl_4 septal fibrosis and the BDL biliary fibrosis models, to demonstrate MAGL expression in this study.
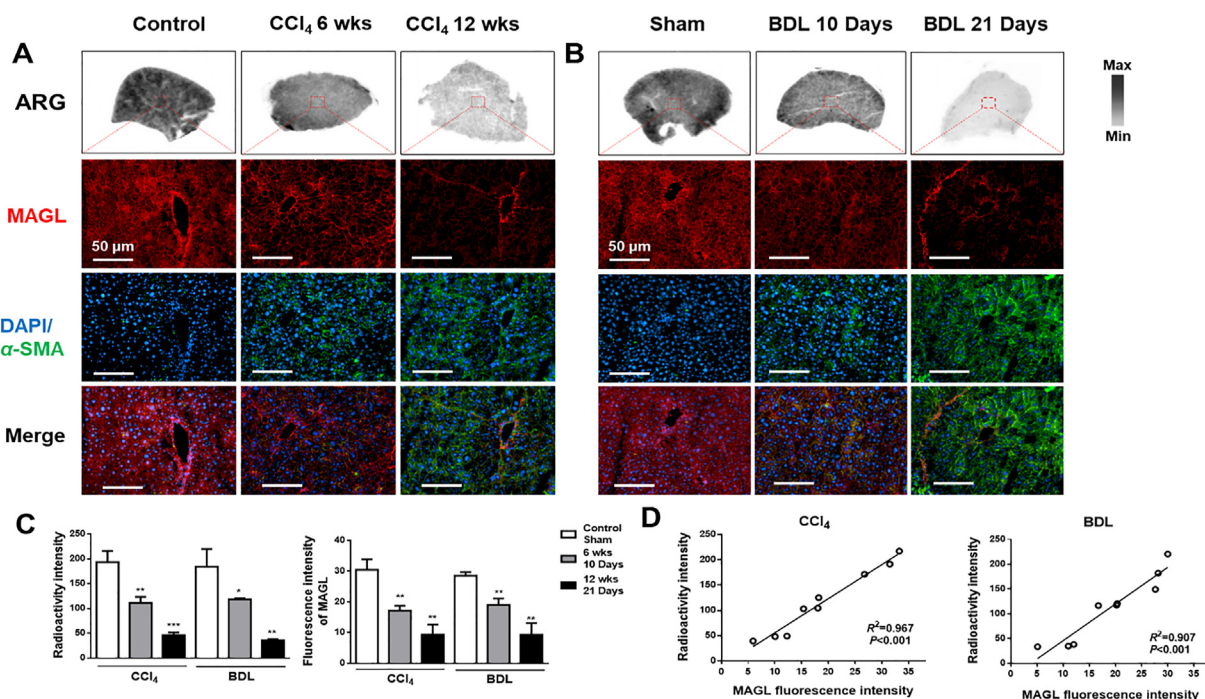
Figure 4 *In vitro* [18F]MAGL-4-11 autoradiographic and MAGL immunofluorescent analysis of liver sections from CCl₄ and BDL mice. (A) Representative autoradiogram of [18F]MAGL-4-11 and double immunohistochemistry of MAGL (red) and α-SMA (green) in CCl₄ liver sections. (B) Representative autoradiographic [18F]MAGL-4-11 images and double immunohistochemistry of MAGL (red) and α-SMA (green) in BDL liver sections. (C) Radioactivity and MAGL fluorescence intensity in CCl₄ and BDL mice liver sections. Graph represents mean ± SEM. *$P < 0.05$, **$P < 0.01$, and ***$P < 0.001$, $n = 3$ animal/group. (D) Correlation between MAGL expression and [18F]MAGL-4-11 uptake in CCl₄ and BDL mice liver sections, $n =$ three animal/group.

Continuous administration of CCl₄ induces toxin-mediated experimental liver fibrosis[20,21], while BDL mimics cholestatic liver injury and biliary fibrosis in patients[22]. Given that CCl₄ and BDL models produce effects through distinct mechanisms, we asked whether MAGL gene/protein expression corresponded with disease pathological severity in each of these fibrotic models, and whether we could measure these changes noninvasively though PET imaging. [18F]MAGL-4-11 is a specific PET ligand for imaging MAGL recently developed by our group[14] and is evaluated in liver fibrosis models in this work.

Here we demonstrated [18F]MAGL-4-11 PET imaged MAGL levels correlated well with mild and severe fibrosis stages in two models, which demonstrated reduced PET signals in early stages of fibrosis and further significantly decreased with disease
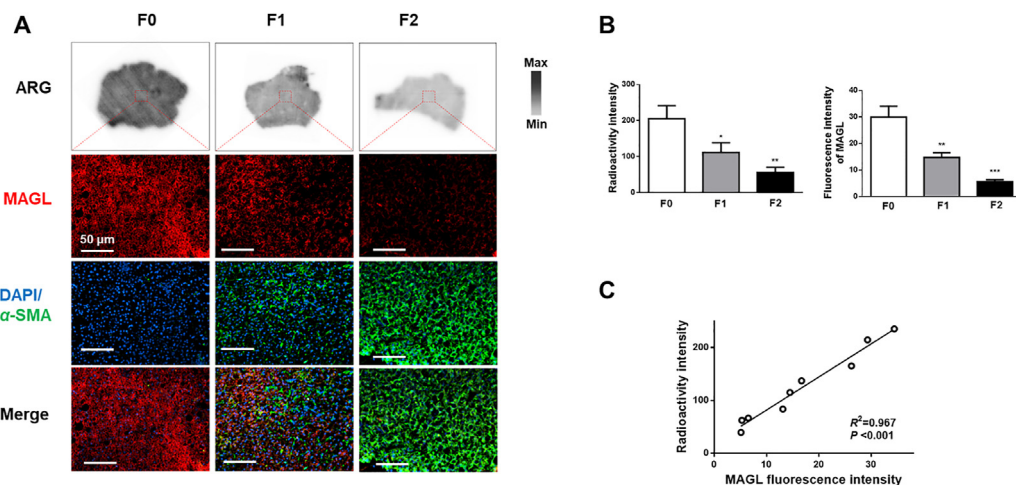

Figure 5 *In vitro* [18F] MAGL-4-11 autoradiography and distribution of MAGL with liver sections of human fibrotic patients. (A) Representative autoradiographic [18F] MAGL-4-11 images and double immunohistochemistry of MAGL (red) and α-SMA (green) in subjects with no, mild and severe fibrosis. (B) Radioactivity and MAGL fluorescence intensity in human liver sections. (C) Correlation between *ex vivo* liver uptake of [18F]MAGL-4-11 and liver MAGL expression in human liver sections, $n =$ three human/group.

progression compared with control mice. Nonspecific uptake in surrounding tissues (such as muscle, heart, and bone) was similar and low in both fibrotic and control mice. Characteristic high accumulation was also identified in brown adipose tissue (BAT) and kidneys, in agreement with the tissue expression of MAGL described in previous studies[23,24] (Supporting Information Fig. S2). *In vitro* autoradiography further supported that [18F] MAGL-4-11 bound specifically to MAGL in fibrotic liver tissue. Collectively, our data indicate that [18F]MAGL-4-11 specifically and accurately reflects MAGL expression and pathological changes in preclinical fibrosis livers. To demonstrate its clinical translation potential, we tested PET ligand [18F]MAGL-4-11 in fibrotic human liver tissue in a variety of clinical stages by autoradiography, and correlated ligand uptake with immunofluorescence staining for MAGL and α-SMA. These studies confirm the specificity of [18F]MAGL-4-11 for MAGL in fibrotic human liver. This is the first time that we demonstrate MAGL expression decreases proportionally with fibrotic stages in human tissue and confirm that our PET imaging marker was sensitive and specific for detection of MAGL level changes.

Previous published studies demonstrated MAGL is a crucial target in liver inflammation and fibrosis[25]. In the present study, we found MAGL expression decreases with fibrosis severity, while its levels in normal liver tissue are high. As another EC degradative enzyme, FAAH revealed a similar pattern of downregulation with MAGL, which is consistent with previous reports in CCl_4 and BDL models[9,10]. In contrast, the EC synthetic enzymes NAPE-PLD and DAGL are enhanced in these different fibrosis models. These increased EC enzymes are associated with robust increases in expression of CB1 receptors, which mediate profibrotic effects[6]. Recently, several research groups have independently identified and evaluated the therapeutic effects of MAGL-targeted treatment in liver injury/inflammation and fibrosis[11−13] *via* enhancement of endocannabinoid signaling and/or suppressing inflammatory eicosanoid production. In light of the ability of [18F]MAGL-4-11 PET to accurately characterize MAGL biological activity *in vivo*, we have confidence that PET imaging will not only enable the detection and identification of molecular changes of MAGL associated with fibrosis progression, but also substantially improve our mechanistic understanding of this important degrading enzyme in liver pathology to assist drug discovery of MAGL-based therapeutics. Although the present study suggests promise for human use, *in vivo* [18F]MAGL-4-11 PET imaging has been limited to small animal experimental models, has not yet entered into clinical application, and will therefore require further refinement.

5. Conclusions

In summary, our PET ligand [18F]MAGL-4-11 shows excellent sensitivity and specificity for MAGL visualization *in vivo* and accurately reflects the histological stages of liver fibrosis in preclinical models and human liver tissues. Further development and validation are warranted to explore the translational value of MAGL-PET imaging *in vivo* in clinical liver fibrosis progression and to facilitate drug discovery towards MAGL-targeted therapeutic for liver disease.

Acknowledgments

Author contributions

Tuo Shao designed the study, performed experiments and wrote manuscript, Zhen Chen and Jian Rong provided radiotracers, Vasily Belov provided imaging analysis supports, Jiahui Chen, Andre Jeyarajan, Xiaoyun Deng, Hualong Fu, Qingzhen Yu, Steve Rwema, Wenyu Lin, and Mikhail Papisov provided experiments supports, Lee Josephson provided writing supports, Raymond T. Chung and Steven H. Liang conceived project, designed the study.

Conflicts of interest

The authors have no conflicts of interest to declare.

Appendix A.   Supporting information

Supporting information to this article can be found online at https://doi.org/10.1016/j.apsb.2021.07.007.

References

1. Bataller R, Brenner DA. Liver fibrosis. *J Clin Invest* 2005;**115**: 209−18.
2. Friedman SL. Liver fibrosis—from bench to bedside. *J Hepatol* 2003; **38**:S38−53.
3. Shao T, Josephson L, Liang SH. PET/SPECT molecular probes for the diagnosis and staging of nonalcoholic fatty liver disease. *Mol Imag* 2019;**18**. 1536012119871455.
4. Shao T, Chen Z, Belov V, Wang X, Rwema SH, Kumar V, et al. [18F]-Alfatide PET imaging of integrin $\alpha v \beta 3$ for the non-invasive quantification of liver fibrosis. *J Hepatol* 2020;**73**:161−9.
5. Mallat A, Teixeira-Clerc F, Lotersztajn S. Cannabinoid signaling and liver therapeutics. *J Hepatol* 2013;**59**:891−6.
6. Teixeira-Clerc F, Julien B, Grenard P, Tran Van Nhieu J, Deveaux V, Li L, et al. CB1 cannabinoid receptor antagonism: a new strategy for the treatment of liver fibrosis. *Nat Med* 2006;**12**:671−6.
7. Julien B, Grenard P, Teixeira-Clerc F, Van Nhieu JT, Li L, Karsak M, et al. Antifibrogenic role of the cannabinoid receptor CB2 in the liver. *Gastroenterology* 2005;**128**:742−55.
8. DeLeve LD, Wang X, Kanel GC, Atkinson RD, McCuskey RS. Prevention of hepatic fibrosis in a murine model of metabolic syndrome with nonalcoholic steatohepatitis. *Am J Pathol* 2008;**173**:993−1001.
9. Giannone FA, Baldassarre M, Domenicali M, Zaccherini G, Trevisani F, Bernardi M, et al. Reversal of liver fibrosis by the antagonism of endocannabinoid CB1 receptor in a rat model of CCl_4-induced advanced cirrhosis. *Lab Invest* 2012;**92**:384−95.
10. Siegmund SV, Seki E, Osawa Y, Uchinami H, Cravatt BF, Schwabe RF. Fatty acid amide hydrolase determines anandamide-induced cell death in the liver. *J Biol Chem* 2006;**281**:10431−8.
11. Habib A, Chokr D, Wan J, Hegde P, Mabire M, Siebert M, et al. Inhibition of monoacylglycerol lipase, an anti-inflammatory and anti-fibrogenic strategy in the liver. *Gut* 2019;**68**:522−32.
12. Cao Z, Mulvihill MM, Mukhopadhyay P, Xu H, Erdelyi K, Hao E, et al. Monoacylglycerol lipase controls endocannabinoid and eicosanoid signaling and hepatic injury in mice. *Gastroenterology* 2013;**144**: 808−17.e15.
13. Tardelli M, Bruschi FV, Fuchs CD, Claudel T, Auer N, Kunczer V, et al. Monoacylglycerol lipase inhibition protects from liver injury in mouse models of sclerosing cholangitis. *Hepatology* 2020;**71**:1750−65.
14. Tardelli M, Bruschi FV, Claudel T, Fuchs CD, Auer N, Kunczer V, et al. Lack of monoacylglycerol lipase prevents hepatic steatosis by favoring lipid storage in adipose tissue and intestinal malabsorption. *J Lipid Res* 2019;**60**:1284−92.
15. Chen Z, Mori W, Deng X, Cheng R, Ogasawara D, Zhang G, et al. Design, synthesis, and evaluation of reversible and irreversible

monoacylglycerol lipase positron emission tomography (PET) tracers using a "tail switching" strategy on a piperazinyl azetidine skeleton. *J Med Chem* 2019;**62**:3336−53.

16. Shao T, Zhao C, Li F, Gu Z, Liu L, Zhang L, et al. Intestinal HIF-1alpha deletion exacerbates alcoholic liver disease by inducing intestinal dysbiosis and barrier dysfunction. *J Hepatol* 2018;**69**:886−95.

17. Siegmund SV, Schwabe RF. Endocannabinoids and liver disease. II. Endocannabinoids in the pathogenesis and treatment of liver fibrosis. *Am J Physiol Gastrointest Liver Physiol* 2008;**294**:G357−62.

18. Grabner GF, Zimmermann R, Schicho R, Taschler U. Monoglyceride lipase as a drug target: at the crossroads of arachidonic acid metabolism and endocannabinoid signaling. *Pharmacol Ther* 2017;**175**:35−46.

19. Hellerbrand C. Inhibition of monoacylglycerol lipase for the treatment of liver disease: tempting but still playing with fire. *Gut* 2018;**68**:382−4.

20. Grasedyck K, Lindner J. Chronic thioacetamide poisoning as a model for experimental liver cirrhosis. *Verh Dtsch Ges Inn Med* 1976;**82**:374−6.

21. Geerts A, Schellinck P, Bouwens L, Wisse E. Cell population kinetics of Kupffer cells during the onset of fibrosis in rat liver by chronic carbon tetrachloride administration. *J Hepatol* 1988;**6**:50−6.

22. Taillandier J, Dumont M, Mesa V, Degott C, Erlinger S. An increase of choleresis in secondary biliary cirrhosis in rats is caused by bile duct secretion. *Gastroenterol Clin Biol* 1990;**14**:313−8.

23. Dinh TP, Carpenter D, Leslie FM, Freund TF, Katona I, Sensi SL, et al. Brain monoglyceride lipase participating in endocannabinoid inactivation. *Proc Natl Acad Sci U S A* 2002;**99**:10819−24.

24. Zimmermann R, Strauss JG, Haemmerle G, Schoiswohl G, Birner-Gruenberger R, Riederer M, et al. Fat mobilization in adipose tissue is promoted by adipose triglyceride lipase. *Science* 2004;**306**:1383−6.

25. Chang JW, Niphakis MJ, Lum KM, Cognetta 3rd AB, Wang C, Matthews ML, et al. Highly selective inhibitors of monoacylglycerol lipase bearing a reactive group that is bioisosteric with endocannabinoid substrates. *Chem Biol* 2012;**19**:579−88.